

A deep *ROSAT* survey - XIV. X-ray emission from faint galaxies

O. Almaini,¹ T. Shanks,² R.E. Griffiths,³ B.J. Boyle,⁴ N. Roche,⁵
G.C. Stewart,⁶ and I. Georgantopoulos⁵

¹*Institute of Astronomy, Madingley Road, Cambridge, CB3 0HA*

²*Department of Physics, University of Durham, South Road, Durham, DH1 3LE*

³*Department of Physics, Carnegie Mellon University, 5000 Forbes Ave., Pittsburgh, PA 15213, USA*

⁴*Anglo-Australian Observatory, PO Box 296, Epping, NSW2121, Australia*

⁵*Johns Hopkins University, Homewood Campus, Baltimore MD21218, USA.*

⁶*Department of Physics, University of Leicester, University of Leicester, LE1 7RH*

MNRAS Submitted 1997 March 4

ABSTRACT

We present a cross-correlation analysis to constrain the faint galaxy contribution to the cosmic X-ray background (XRB). Cross-correlating faint optical galaxy catalogues with unidentified X-ray sources from 3 deep *ROSAT* fields we find that $B < 23$ galaxies account for $20 \pm 7\%$ of all X-ray sources to a flux limit of $S(0.5 - 2.0 \text{ keV}) = 4 \times 10^{-15} \text{ erg s}^{-1} \text{ cm}^{-2}$. To probe deeper, galaxies are then cross-correlated with the remaining unresolved X-ray images. A highly significant signal is obtained on each field. Allowing for the effect of the *ROSAT* point-spread function, and deconvolving the effect of galaxy clustering, we find that faint $B < 23$ galaxies directly account for $23 \pm 3\%$ of the unresolved XRB at 1 keV. Using the optical magnitude of faint galaxies as probes of their redshift distribution, we find evidence for strong evolution in their X-ray luminosity, parameterised with the form $L_x \propto (1+z)^{3.22 \pm 1.0}$. Extrapolation to $z = 2$ will account for $40 \pm 10\%$ of the total XRB at 1 keV.

Key words: galaxies: evolution - X-rays:general - X-rays: galaxies - diffuse radiation
X-rays: general

1 INTRODUCTION

The nature and origin of the cosmic X-ray background remains a major unsolved problem. The most significant progress has been made in the soft X-ray band below 3 keV since the launch of high resolution imaging satellites such as *Einstein* and *ROSAT*. By resolving as many sources as possible in the deepest exposures *ROSAT* exposures (Hasinger et al. 1993) up to 70% of the 0.5 – 2 keV XRB has now been resolved into discrete sources.

Using a survey of 7 deep (21–57ks) *ROSAT* fields we have detected over 400 X-ray sources above a 4σ threshold to an approximate flux limit of $S(0.5 - 2.0 \text{ keV}) \sim 4 \times 10^{-15} \text{ erg s}^{-1} \text{ cm}^{-2}$. By optical spectroscopy we then identify the optical counterparts to these X-ray sources. This technique has shown that broad-line QSOs directly account for at least 30% of the total 0.5 – 2 keV XRB flux (Shanks et al. 1991). As a larger sample of QSOs became established, detailed studies of the QSO X-ray luminosity function (Boyle et al. 1994) and the source number count distribution (Georgantopoulos et al. 1996) have shown that QSOs

are unlikely to contribute more than 50% of the XRB at 1 keV. The existence of a new X-ray emitting population was postulated.

A further problem in explaining the XRB with QSOs is the shape of their X-ray spectra. QSOs show relatively steep X-ray spectra with indices of $\Gamma = 2.2 \pm 0.1$ while the 1 – 10 keV XRB has a significantly flatter spectrum with $\Gamma = 1.4$ (Gendreau et al 1995). Deep *ROSAT* surveys have begun to resolve a population of harder X-ray sources at the faintest flux limits (Hasinger et al. 1993, Vikhlinin et al. 1995, Almaini et al. 1996). There have been suggestions that this hardening may be due to a change in the intrinsic properties of QSOs at high redshift or the effect of intervening photoelectric absorption (Morisawa & Takahara 1990, Vikhlinin et al. 1995) but recent work by Almaini et al. (1996) found no significant change in the 0.5 – 2 keV X-ray spectra of QSOs with flux or redshift. The spectral hardening is due to another, unidentified X-ray population. Many of these unidentified X-ray sources appear to be associated with faint galaxies. In particular, a number of individually identified narrow-emission line galaxies show spectra signif-

icantly harder than QSOs, more consistent with the spectrum of the XRB (Almaini et al. 1996). Similar results were obtained by Carballo et al. (1995) and Romero-Colmenero (1996).

It is becoming clear that X-ray emission from galaxies can make a significant contribution to the XRB. Using *Einstein* observations of local galaxies, Giacconi et al. (1987) extrapolated the observed X-ray to optical flux ratios to the faintest ($B < 27.5$) optical counts of Tyson et al. (1988) and found that normal galaxies could produce at least 13% of the XRB at 2 keV. Griffiths and Padovani (1990) used the observed evolution in the $60\mu\text{m}$ luminosity of IRAS galaxies and the local X-ray to infra-red ratios to estimate that IRAS and starburst galaxies seen to high redshift could produce 10-30% of the 0.5-3 keV XRB.

Other studies have probed the galaxy contribution using the two-point cross-correlation between the hard (2-10 keV) XRB and various optical and infra-red galaxy catalogues (Lahav et al. 1993, Miyaji et al. 1994, Carrera et al. 1995, Refregier et al. 1997). These galaxy catalogues were generally fairly shallow ($z < 0.1$) but by correcting for the effects of clustering and extrapolating the measured volume emissivity to $z \sim 5$ it was shown that 10-30% of the XRB could be explained by sources associated with galaxies. However because of the unknown error in such an extrapolation and the uncertain evolutionary properties of galaxies it is clearly desirable to probe more distant objects directly. The clearest evidence that fainter galaxies could be important contributors to the XRB came from the study of Roche et al (1995). Using the improved sensitivity and angular resolution of the *ROSAT* satellite they were able to probe fainter limits and much smaller angular scales ($\sim 15''$). By cross-correlating faint galaxy catalogues with X-ray sources they obtained a $2 - 3\sigma$ detection implying that $B < 21$ galaxies account for $\sim 5\%$ of the X-ray sources. However they obtained a more significant ($\sim 5\sigma$) signal by removing the X-ray sources and cross-correlating with 3 deep (21-49ks) images of the *unresolved* XRB. The results implied that galaxies to a limit of $B = 23$ directly contribute $\simeq 17\%$ of the 1 keV XRB. A simple extrapolation to $B < 28$ showed that galaxies could account for $\sim 30\%$ of the XRB or possibly more with evolution. Similar results have since been obtained on another field in the work of Roche et al. (1996b).

In this paper we perform an independent test of these results on 2 new deep ($\sim 50\text{ks}$) *ROSAT* exposures. The deepest field (GSGP4) from the Roche et al. (1995) work is also included, but this time the effect of clustering is analysed more rigorously. First we will perform a cross-correlation of the unidentified X-ray sources with faint galaxies. We will then probe deeper into the remaining unresolved XRB. To deconvolve the effect of galaxy clustering we will make use of the method developed by Treyer & Lahav (1996) (hereafter TL96), extending their formalism to take account of the *ROSAT* point spread function. We will then consider the cross-correlation signal as a function of magnitude to obtain an estimate of the evolution of X-ray emissivity with redshift.

2 CROSS-CORRELATING X-RAY SOURCES WITH FAINT GALAXIES

Field	RA	DEC	N_H	Exposure
BJS855	10 ^h 46 ^m 24 ^s	−00°21′00″	2.9 ± 0.4	57147s
BJS864	13 ^h 43 ^m 43 ^s	−00°15′00″	2.6 ± 0.3	52466s
GSGP4	00 ^h 57 ^m 29 ^s	−27°38′13″	1.8 ± 0.3	48995s

Table 1. Summary of deep *ROSAT* fields, with coordinates in J2000 and galactic column density in $10^{20} \text{ atom cm}^{-2}$.

2.1 Data and method

In this paper we use 3 deep *ROSAT* PSPC exposures with optical identifications from the X-ray source catalogue of Shanks et al. (1997). We refer to this catalogue paper for full details of the X-ray source detection and optical follow-up observations. To a flux limit of $S(0.5 - 2.0 \text{ keV}) \sim 4 \times 10^{-15} \text{ erg s}^{-1} \text{ cm}^{-2}$, approximately 50% of the X-ray sources were identified as QSOs by optical spectroscopy (Boyle et al. 1994). Many of the remaining X-ray sources had no obvious QSO candidate within their error box, but appeared to be associated with faint galaxies on deep photographic plates (Georgantopoulos et al. 1996). Due to the high surface density of galaxies at faint magnitudes however ($\sim 10000 \text{ deg}^{-2}$ at $B < 23$, Metcalfe et al. 1995) and the relatively large X-ray error circle ($\sim 25''$ FWHM) many of these will be chance associations. If we look deep enough we can find a galaxy counterpart to any X-ray source. We will therefore adopt a statistical approach to determine the fraction of galaxies among the X-ray sources.

The 3 deepest *ROSAT* fields from the survey will be used in this analysis, including the GSGP4 field analysed by Roche et al. (1995). A summary of these exposure is given in Table 1. The optical galaxy catalogues were obtained from COSMOS plate scans of Anglo-Australian Telescope photographic plates, calibrated with magnitudes and a star-galaxy classification flag. This optical data was previously used for the galaxy clustering and number count analyses of Stevenson et al (1985) and Jones et al. (1991). Further details of the plate reduction and zero point magnitude calibration are given in Jones et al (1991). Astrometric solutions to convert the plate co-ordinates into R.A. and Dec. were already in existence from the UVX QSO survey of Boyle et al. (1990) and Boyle, Jones & Shanks (1991). A second transformation was then required to convert R.A. and Dec. into the (x,y) *ROSAT* pixel coordinates. This was performed using approximately 10-15 bright stars and UVX QSOs with definite counterparts on each *ROSAT* image. These gave 6 coefficient astrometric transforms with rms positional errors of between 7.1 and 8.4 arcseconds, as expected given the angular resolution of the *ROSAT* PSPC. On Figure 1 we show the resulting positions of $B < 23$ galaxies on one of the fields (BJS855) in X-ray coordinates. The plate edges and larger plate holes are clearly visible, where bad data has been flagged around bright objects or in some case where plate defects were detected in the plate measuring process (Jones et al. 1991).

In calculating the cross-correlation of optical positions with X-ray sources the number of galaxies were counted in successive annuli of $5''$ width around each X-ray source. This distribution was then compared with the counts obtained by placing 50,000 random points over each of the field areas,

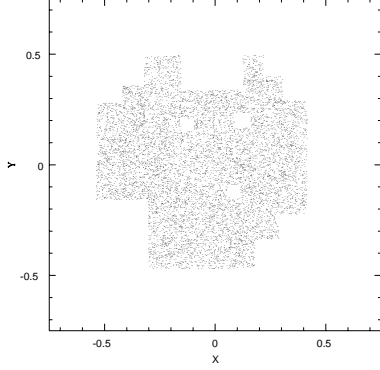


Figure 1. Showing the positions of 8714 galaxies with magnitudes $B < 23$ on the BJS855 field after transformation to X-ray coordinates (scaled to degrees).

taking care to avoid the plate edges and “holes”. A two point cross-correlation function $C_{xo}(\theta)$ of X-ray and optical sources can then be defined as:

$$C_{xo}(\theta_i) = \frac{N_{xo}(\theta_i)N_r}{N_{xr}(\theta_i)N_o} - 1 \quad (1)$$

where, N_r is the total number of random points, N_o the number of optical plate sources being correlated and $N_{xo}(\theta_i)$ and $N_{xr}(\theta_i)$ give the number of X-ray/optical and X-ray/random pairs respectively.

2.2 Results

Removing only the X-ray sources identified with QSOs or galactic stars we cross-correlate the positions of the remaining 149 unidentified 4σ sources with the objects classified as galaxies on photographic plates. These optical galaxies were split into a bright sample with $B < 21$ and a fainter sample with $21 \leq B \leq 23$. The results are shown in Table 2, where we display the number of galaxies found within $30''$ of an X-ray source compared to the distribution expected by chance. A $30''$ radius approximately corresponds to the 3σ ROSAT PSPC positional error.

Considering first the cross correlation with brighter $B < 21$ galaxies, on each field we find an excess compared to a random distribution. Overall we find 52 source-galaxy pairs compared to 31.5 expected by chance, amounting to a 3.7σ rejection of the null hypothesis that the two distributions are not correlated. This would indicate an excess of $\approx 20.5 \pm 7.2$ $B < 21$ galaxies around X-ray sources. On Figure 2(a) we display the source-galaxy cross-correlation in $15''$ radial bins.

To probe deeper, we repeat the cross-correlation with the ~ 5000 fainter galaxies in the magnitude range $21 \leq B \leq 23$. We find 326 galaxies within $30''$ of an X-ray source compared to 278 expected. This represents a 2.9σ rejection of the hypothesis of no correlation and indicates an excess of $\approx 48 \pm 17$ of these fainter galaxies around X-ray sources. The cross-correlation function is displayed in Figure 2(b) for the 3 fields combined.

We must now make a correction for the effect of galaxy

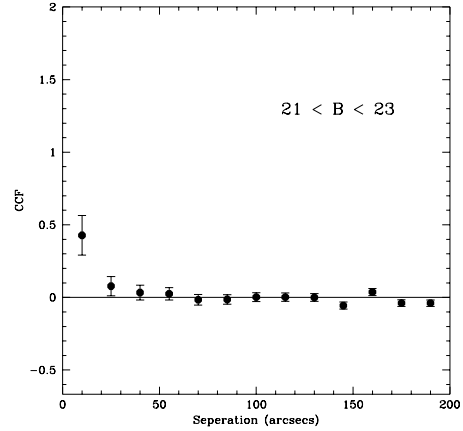
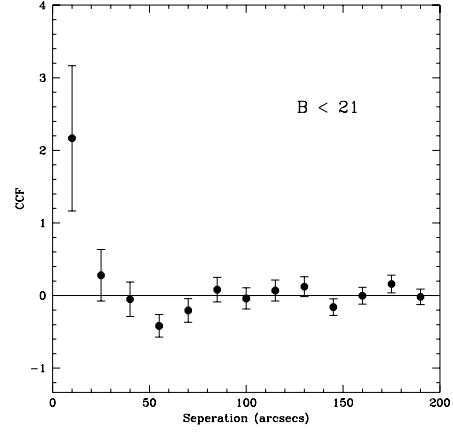


Figure 2. (a) The cross-correlation function $C_{xo}(\theta)$ of unidentified X-ray sources from 3 deep fields with $B < 21$ mag galaxies. On (b) we repeat the analysis with fainter $21 \leq B \leq 23$ mag galaxies. Note the change in scale compared to (a). Error bars are due to \sqrt{N} statistics.

clustering. Since galaxies are clustered on the scales probed by this analysis this can enhance the excess of source-galaxy pairs. We therefore apply a simple correction based on $\omega_{gg}(\theta)$, the angular autocorrelation function of faint galaxies (from Roche et al 1996a). Defining $\Delta N'_{gx}(\theta)$ to be the observed excess of source-galaxy pairs measured within a given angle θ , this will be enhanced relative to the true number of X-ray emitting galaxies $\Delta N_{gx}(\theta)$ such that:

$$\Delta N_{gx}(\theta) = \frac{\Delta N'_{gx}(\theta)}{1 + G_{tot}^{-1} \Delta N_{gg}(\theta)} \quad (2)$$

where $\Delta N_{gg}(\theta)$ is the excess of galaxies within angle θ compared to a random distribution, obtained by integration of $\omega_{gg}(\theta)$, and G_{tot} is the total number of galaxies in the entire image. For the brighter $B < 21$ galaxies this gives a 25% clustering enhancement within a radius of $30''$. At $21 < B < 23$ the effect is slightly more significant, accounting for 31% of the excess signal.

Thus overall, allowing for the effects of clustering, we

Magnitude range	Field	Pairs < 30''	Expected	Excess significance
$B < 21$	GSGP4	22	13.2	2.4σ
	BJS855	19	12.3	1.9σ
	BJS864	11	5.93	2.1σ
	Total	52	31.5	3.7σ
$21 \leq B \leq 23$	GSGP4	123	104.9	1.8σ
	BJS855	101	85.0	1.7σ
	BJS864	102	88.1	1.5σ
	Total	326	278	2.9σ

Table 2. Showing the number of faint galaxies found within 30'' of unidentified X-ray sources on 3 deep fields compared to the number expected by chance. The galaxies are split into those with $B < 21$ and fainter galaxies with $21 \leq B \leq 23$.

have evidence that $\simeq 48 \pm 17$ of the 149 unidentified X-ray sources are due to galaxies with $B < 23$, strengthening the initial findings of Roche et al (1995). Hence from a total of 236 sources on 3 deep fields we have shown that faint ($B < 23$) galaxies contribute $\sim 20 \pm 7\%$ of the total source counts to a flux limit of $S(0.5 - 2.0\text{keV}) \sim 4 \times 10^{-15} \text{erg s}^{-1} \text{cm}^{-2}$.

However when we scale this 20% galaxy contribution by the median flux of the unidentified X-ray sources ($\sim 7 \times 10^{-15} \text{erg s}^{-1} \text{cm}^{-2}$) we obtain a total contribution of $1.2 \pm 0.4 \times 10^{-9} \text{erg s}^{-1} \text{cm}^{-2} \text{sr}^{-1}$ which accounts for only $\sim 4\%$ of the total XRB. We will therefore attempt to probe much deeper in Section 3 by cross-correlating with the remaining *unresolved* XRB.

3 CROSS-CORRELATING THE UNRESOLVED X-RAY BACKGROUND WITH FAINT GALAXIES

3.1 The data

In this section we extend the cross-correlation technique to probe the remaining unresolved component of the cosmic X-ray background and thus investigate the origin of X-ray emission beyond the limit of significant source detection. By performing the analysis with different magnitude slices of the galaxy sample we may also be able to deduce the redshift evolution of X-ray emissivity from faint galaxies.

The X-ray images were obtained from deep ($\sim 50\text{ks}$) *ROSAT* observations reduced using the STARLINK *Asterix* X-ray data reducing package. Since the X-ray background below 0.5keV is dominated by galactic emission and solar scattered X-rays (Snowden & Freyberg 1993) the images used in the cross-correlation are extracted from only the $0.5 - 2\text{keV}$ data. Data from periods of high particle background were also removed from the analysis, excluding approximately 10% of the photons when the Master Veto Rate was above $170 \text{ counts s}^{-1}$ (Plucinsky et al. 1993). Additional data was available for the BJS855 and BJS864 fields from serendipitous pointings obtained from the *ROSAT* data archive, offset 6 and 7 arcminutes respectively from the original field centres and providing an additional $\sim 20\text{ks}$ of data. This data was processed separately before a mosaic of the final images was produced. The 4σ sources were then removed from the data using a range of exclusion radii suitable for excluding 98% of the photons, depending on the off-axis angle of the source. This radius varied from $30.6''$

for a source on axis to $75.6''$ for a source at a radius of 20 arcminutes. Inspection of the resulting images revealed that only one source showed evidence for being extended and could not be successfully removed in this way. This source, GSGP4X:032, was identified as a distant ($z = 0.56$) galaxy cluster. A 70% larger radius was required to successfully remove this source. Finally, only the central 16 arcminute regions were used in the cross-correlation analysis since the sensitivity of the PSPC drops off rapidly beyond 20 arcminutes (Hasinger et al. 1992). For the BJS855 and BJS864 fields, where deeper exposures have been obtained by adding additional archive data, only regions of the final image lying within 16 arcminutes of *both* field centres are used.

3.2 Cross-correlation results

A two point cross-correlation between the unresolved X-ray images and the faint galaxy catalogues was obtained by counting the number of X-ray photons in successive annuli around each galaxy and comparing this with the mean pixel intensity. By repeating for every galaxy in the field (avoiding holed regions), the cross-correlation is defined by:

$$W_{xg}(\theta_i) = \frac{\sum N_x(\theta_i)}{\sum N_p(\theta_i) \langle N_X \rangle} - 1 \quad (3)$$

where $N_x(\theta_i)$ and $N_p(\theta_i)$ are the total number of X-ray photons and pixels respectively within annulus i of each galaxy, $\langle N_X \rangle$ is the mean number of photons per pixel and the summations occur over all the galaxies in the field. Error estimates were obtained by splitting each field into 4 quadrants and obtaining the cross-correlation for each separately. The error on W_{xg} was then estimated from the error on the mean from these quadrants.

The resulting two point cross-correlations between faint $18 < B < 23$ galaxies and the unresolved XRB are shown in Figure 3 in $15''$ bins. It is clear that a significant positive signal has been detected on each field. The errors on the first two bins alone ($< 30''$) suggest individual detections $> 3\sigma$ significance. The independent analysis of the GSGP4 field is seen to be in excellent agreement with the results of Roche et al. (1995). Thus we find further strong evidence that faint galaxies are not only significant contributors to the resolved X-ray source counts but also to the fainter, as yet unresolved component of the X-ray background. In Table 3 we show the number of galaxy-photon pairs within $30''$

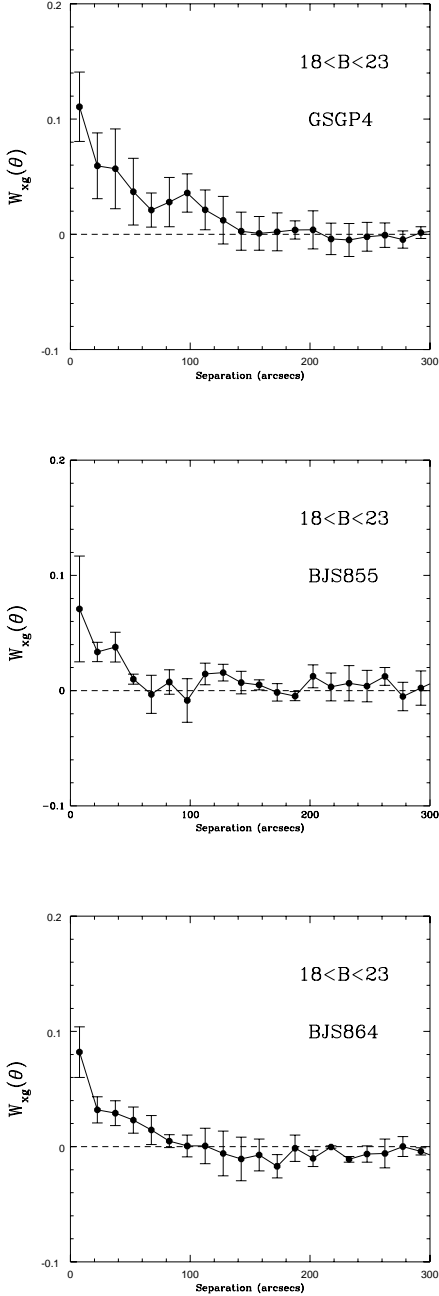


Figure 3. The cross-correlation function $W_{xg}(\theta)$ of the unresolved $0.5 - 2\text{keV}$ X-ray background with faint $18 \leq B \leq 23$ galaxies on 3 deep fields.

of the galaxies compared to the counts expected from a random distribution. The excess X-ray photons close to galaxies suggest $> 3.5\sigma$ detections on each field assuming Poisson statistics. We have clearly confirmed the initial findings of Roche et al. (1995).

In Figure 4 we show W_{xg} for the 3 deep fields combined, where we have summed galaxy-photon pairs across all fields and calculated the expected counts by combining the 3 separate $\sum N_p(\theta_i) \langle N_X \rangle$ terms. Errors have been estimated in the same manner as before by calculating 4 cross-

Field	Photons $< 30''$	Expected	Excess significance
GSGP4	8575	8154	4.7
BJS855	5763	5490	3.7
BJS864	7771	7414	4.1
Total	22109	21058	7.2

Table 3. Results of the cross-correlation of $18 \leq B \leq 23$ catalogue galaxies with the unresolved $0.5 - 2.0\text{keV}$ X-ray background on 3 deep fields, comparing the number of $0.5 - 2.0\text{keV}$ X-ray photons found within $30''$ with a random distribution.

correlations from the quadrants of each field and using the error on the mean values of W_{xg} .

3.3 The effect of galaxy clustering

We have established a highly significant cross-correlation between the unresolved component of the cosmic XRB and faint galaxies. Galaxies do not randomly sample the sky however and are well known to show evidence of clustering and structure on the scales probed by our analysis. It is therefore probable that a non-negligible fraction of the enhanced signal in the cross-correlation is due to the clustering of galaxies with each other. In effect, the galaxies will correlate with the emission of their neighbours as well. One approach (see Roche et al. 1995) is to apply an approximate correction using the *angular* clustering of the observed optical galaxies. However this will not account for the X-ray emission arising from fainter unseen objects ($B > 23$) which may be clustered with the galaxy catalogue. This effect is discussed in detail in the work of TL96, where a prescription for modelling these populations is presented. We will now apply this formalism to our data, taking care to allow for the effect of the *ROSAT* PSFC point-spread-function (PSF). This effect was neglected by TL96. A detailed description of the effect of the PSF can be found in Refregier et al. (1997).

3.4 Correlation functions and the effect of the PSF

Under the assumption that the XRB arises from discrete, point-like X-ray sources, it has been shown that two terms will contribute to the cross-correlation of faint galaxies with the X-ray background (Lahav 1992, Treyer & Lahav 1995, Refregier et al. 1997).

$$\eta_0 = \eta_p + \eta_c. \quad (4)$$

For the ideal case of a delta-function PSF with cell sizes $\omega \rightarrow 0$, this function is related to the normalized form of W_{xg} (Equation 3) by:

$$W_{xg}(\theta) = \frac{\eta_0}{\omega^2 \bar{I} \bar{N}} \quad (5)$$

In this expression \bar{I} is the mean intensity of the unresolved XRB and \bar{N} gives the number of catalogue galaxies per steradian. The η_p term comes from the direct contribution from the catalogue galaxies themselves. This is known as the *Poisson* term, which in the idealized case only exists

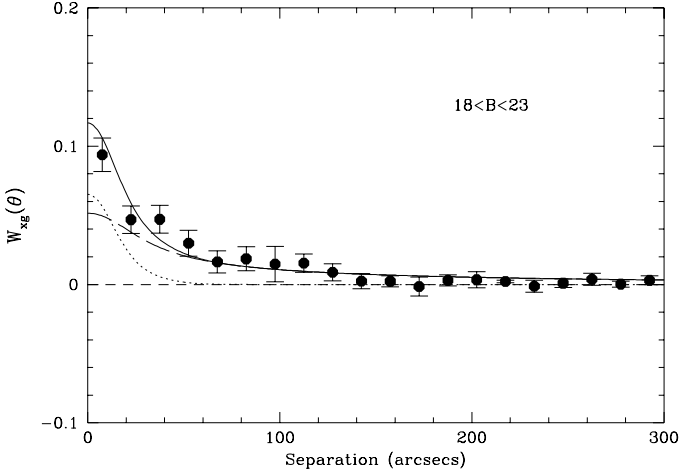


Figure 4. The total cross-correlation function $W_{xg}(\theta)$ of the unresolved $0.5 - 2.0$ keV X-ray background on 3 deep *ROSAT* fields with $18 \leq B \leq 23$ galaxies. Also shown is the best fitting model of the form given in Equation 14, formed as the sum of the Poisson term (dotted line) and a clustering term (dashed line).

at zero lag ($\theta = 0$). For cells of solid angle ω this term is directly related to the X-ray intensity $\Delta \bar{I}_g$ contributed by the galaxies such that:

$$\eta_p = \omega \Delta \bar{I}_g = \omega \int_z \frac{\rho_g(z)}{4\pi r_l^2} dv(z). \quad (6)$$

where we define $\rho_g(z)$ as the observed volume emissivity of the galaxy population, $dv(z)$ is the volume element per unit angle and r_l is the luminosity distance.

The second term η_c arises from the clustering of the X-ray sources with the galaxy population and is known as the *clustering* term. Treyer & Lahav (1996) have calculated the theoretical angular cross-correlation of a galaxy population with the X-ray background. They find that the clustering term η_c obeys a simple power law of the form:

$$\eta_c(\theta) = A_{xg} \theta^{1-\gamma} \quad (7)$$

where the amplitude A_{xg} can in principle be used to evaluate the X-ray volume emissivity due to galaxies given a specific model of their redshift distribution, clustering and luminosity evolution (see Section 3.5). TL96 applied this simple form to the measurements of Roche et al. (1995) to obtain an estimate of the galaxy contribution to the XRB. As we will demonstrate below, fitting this functional form directly to measurements of $W_{xg}(\theta)$ isn't strictly valid due to the effect of *ROSAT* PSF. This has the effect of smearing out the Poisson term to make a significant contribution at non-zero lag. We will discuss how to deconvolve the Poisson and clustering terms in Section 3.6. First we will use the formalism of TL96 and a specific model for the galaxy population to relate the amplitude of the clustering term A_{xg} to the X-ray volume emissivity.

3.5 Modelling the galaxy population

We assume that any diffuse component of the $0.5 - 2.0$ keV XRB is negligible in comparison with the source component and model the observed volume emissivity of the source population using an evolutionary parameter q such that:

$$\rho_{XRB}(z) = \rho_s(z) = \rho_0(1+z)^q \quad (8)$$

Thus the intensity of the XRB per unit solid angle is given by:

$$\bar{I} = \omega \int_z \frac{\rho_s(z)}{4\pi r_l^2(z)} dv(z) \quad (9)$$

We will further assume that the spatial cross-correlation of galaxies with the X-ray sources $\xi(r, z)$ to be the same as the auto-correlation of faint galaxies with themselves.

Next we must characterise the properties of the galaxy population at a given redshift. Deep spectroscopic surveys (eg. Glazebrook et al 1995) have measured the galaxy $N(m, z)$ to optical magnitudes of $B \simeq 24$. We hope to model even deeper than this however. Fainter galaxies lack redshifts, so we will use the latest evolution model of Roche et al. (1996a). This model is consistent with current spectroscopic results (eg. Cowie et al. 1996) and reproduces the faint number count distribution. In general this model predicts a higher redshift distribution for faint blue galaxies than the parametric form of Efstathiou (1995) used in TL96.

Next we must model the clustering properties of the galaxy population and its evolution with redshift. We will adopt the standard form (Peebles 1980):

$$\xi(r, z) = (1+z)^{-(3+\epsilon)} \left(\frac{r}{r_0} \right)^{-\gamma} \quad (10)$$

where the proper coordinate r is the spatial separation between the sources and ϵ models the clustering evolution. We will adopt a stable clustering model ($\epsilon = 0$) and a correlation radius of $r_0 = 4.4 h^{-1} \text{Mpc}$ (Loveday et al. 1995). Using these parameters and the galaxy evolution model described above, Roche et al. (1996a) were able to fit the observed galaxy angular clustering to a magnitude of $B = 27$.

To interpret our observations we will use the framework developed by TL96, who have calculated the theoretical angular cross-correlation of a galaxy population with the X-ray background. The detailed calculations are somewhat cumbersome and will not be repeated here. However they find that the clustering term $\eta_c(\theta)$ obeys a simple power law (Equation 7) where the amplitude is given by:

$$A_{xg} = \frac{\rho_0 r_0^\gamma H_\gamma f(\aleph)}{4\pi} \quad (11)$$

The function H_γ is given by:

$$H_\gamma = \int_{-\infty}^{+\infty} dx (1+x^2)^{-\gamma/2} \quad (12)$$

Assuming the standard $\gamma = 1.8$ leads to $H(\gamma) = 3.68$. Defining a global evolution parameter $\aleph = \gamma - \epsilon + q - 5$, the function $f(\aleph)$ takes the form:

$$f(\aleph) = \int_z dz (1+z)^\aleph r_c^{1-\gamma} \int_{B_{min}}^{B_{max}} N(m, z) dm. \quad (13)$$

where B_{min} and B_{max} represent the magnitude range of the galaxy catalogue.

Thus we may in principle re-arrange Equation 11 to obtain a value for the local X-ray volume emissivity ρ_o using our chosen description of the galaxy population and our observed X-ray parameters \bar{I} and A_{xg} . As discussed above however, measuring A_{xg} is non-trivial since we must deconvolve the effect of the Poisson term. This will be discussed in the next section.

In order to estimate the evolutionary parameter \aleph we need a value for the parameter q which describes the evolution in the *observed* X-ray emissivity of (Equation 8). We will attempt to measure this evolution directly in Section 3.7.

3.6 Deconvolving the Poisson and clustering terms in $W_{xg}(\theta)$

We define the PSF of the *ROSAT* PSPC to be the function $\psi(\theta)$ normalised to unity over the whole sky. We adopt the parametric form given by Hasinger et al. (1995). Our images are extracted from the central 16 arcminute region of the PSPC and we will use the mean weighted PSF over this radius, assuming a mean photon energy of 1keV.

The effect of the *ROSAT* PSF is to smear out the X-ray emission over neighbouring pixels, and hence the Poisson and clustering terms in the cross-correlation, derived assuming a delta function PSF, will be smeared out compared to Equation 5 to produce the measured $W_{xg}(\theta)$ as follows:

$$W_{xg}(\theta) = \frac{1}{\bar{I}N2\pi\omega^4} \int_0^{2\pi} d\phi_{12} \int_{C_1} d\Omega_1 \int_{C_2} d\Omega_2 \times \int_S d\Omega_S \psi(\theta_{2s}) \eta(\theta_{1s}) \quad (14)$$

The $d\Omega_1$ and $d\Omega_2$ integrals are evaluated over cells C_1 and C_2 separated by θ_{12} . A rigorous derivation of such equations can be found in Refregier et al. (1997). The final integral is evaluated over the whole sky, and is effectively a 2-dimensional convolution of the point spread function with the idealized correlation function $\eta(\theta)$.

Although the two terms η_c and η_p both contribute to the observed $W_{xg}(\theta)$ they are not independent. By Equation 6 the Poisson term η_p can be evaluated from the X-ray volume emissivity, which in turn is related to the clustering term η_c via Equations 8 and 11. Therefore $\eta(\theta)$ in the above integral may be replaced by:

$$\eta(\theta) = A_{xg} \left[\theta^{1-\gamma} + \frac{4\pi}{r_o^3 H_\gamma f(\aleph)} \int_z \frac{(1+z)^q}{4\pi r_l^2} dv \right] \quad (15)$$

We must therefore evaluate this functional form of $W_{xg}(\theta)$ numerically and then fit to our observations to obtain an estimate of the amplitude A_{xg} . In order to evaluate this function, however, we must assume a value for the evolutionary parameter q . We will now attempt to measure this evolution directly.

3.7 Constraining evolutionary parameters

The largest uncertainty in previous estimates of the galaxy contribution to the XRB has been the assumed redshift evolution (eg. see Lahav et al. 1993, Roche et al. 1995). Treyer

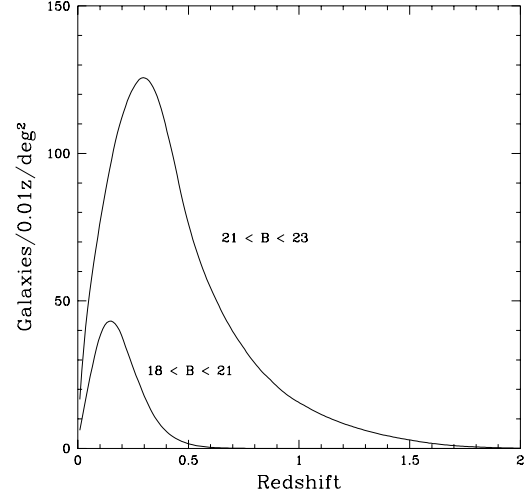


Figure 5. Galaxy redshift distributions predicted using the PLE model of Roche et al. (1996a) for $B < 23$ galaxies split into a ‘bright’ and ‘faint’ sample.

& Lahav (1996) proceed under the assumption that the luminosity ratio L_X/L_{opt} remains constant at all redshifts. To study this assumption further, we consider cross-correlating with successively fainter magnitude slices of the galaxy population. Since fainter galaxies, on average, will probe higher redshifts it should in principle be possible to constrain the redshift evolution of the galaxy population. Modifying Equations 11 and 13 we can obtain theoretical cross-correlations of the unresolved XRB with galaxies between the magnitude limits $[m_1, m_2]$:

$$\delta A_{xg} = \frac{\rho_0 r_o^\gamma H_\gamma}{4\pi \bar{I} \Delta N} \int_z dz (1+z)^\aleph r^{1-\gamma} \int_{m_1}^{m_2} N(m, z) dm \quad (16)$$

We can normalize this by the observed cross-correlation from the full $(18 < B \leq 23)$ galaxy sample, giving:

$$\delta A_{xg} = \frac{A_{xg} \bar{N}}{f(\aleph) \Delta N} \int_z dz (1+z)^\aleph r^{1-\gamma} \int_{m_1}^{m_2} N(m, z) dm \quad (17)$$

Thus by performing the cross-correlation with galaxies in different magnitude ranges we may be able to constrain the evolutionary parameter \aleph and hence the evolution in X-ray emissivity.

The galaxy catalogue was therefore split into “bright” ($18 < B < 21$) and “faint” ($21 \leq B < 23$) subsets. The redshift distributions for these samples are shown in Figure 5, as predicted from the models of Roche et al. (1996a). Two separate cross-correlations with the unresolved XRB are then carried out. The results are displayed in Figure 6. The brighter sample clearly show a higher overall correlation amplitude. To compare with a range of theoretical predictions (in order to constrain the evolution) we evaluate the integral in Equation 17 to obtain expected amplitude A_{xg} as a function of the evolutionary parameter \aleph . These are displayed in Figure 7. Clearly we expect the relative cross-correlation amplitudes to change dramatically depending on

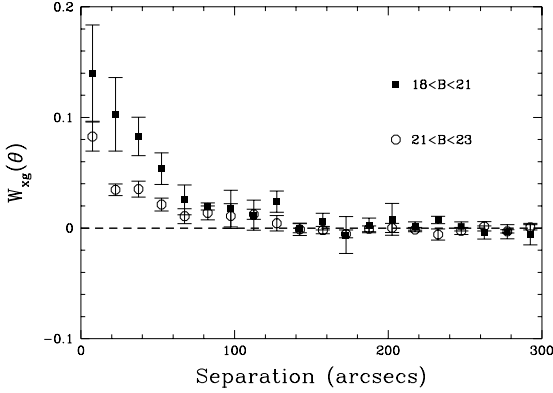


Figure 6. The cross-correlation function $W_{xg}(\theta)$ of galaxies with the unresolved $0.5 - 2.0$ keV XRB from three *ROSAT* fields. The galaxies are split into a bright and faint sample.

the redshift evolution. With stronger evolution, the amplitude for the brighter (more local) sample will decrease.

To constrain \aleph we therefore evaluate δA_{xg} for both galaxy samples. We fit models of the form given by Equations 14 and 15. A complication arises since the functional form we fit requires a value for q in advance (to evaluate the Poisson contribution), so we start with the assumption that $q = 0$ and proceed iteratively. In practice the *relative* amplitudes of the Poisson and clustering terms are fairly insensitive to the assumed value of q and vary by only $\sim 10\%$ with q in the range $q \in [0, 3]$. Nevertheless we start with a value $q = 0$, use the measured amplitude A_{xg} to constrain the evolutionary parameter \aleph (and hence q) and then repeat the process. Within a couple of iterations we converge on values for the amplitudes A_{xg} for both magnitude slices.

With θ measured in radians we obtain amplitudes of $5.15 \pm 0.35 \times 10^{-5}$ for the bright galaxies and $2.8 \pm 0.2 \times 10^{-5}$ for the fainter sample. These amplitudes were obtained by fitting to $W_{xg}(\theta)$ for $\theta < 2$ arcminutes and the errors are derived from the variance in the amplitudes from 3 independent fields. The resulting estimates for the evolutionary parameter \aleph are shown in Figure 7. The shaded area shows the 1σ confidence region on the *observed* amplitude for the brighter galaxies and the corresponding preferred values of \aleph . For the fainter sample however the weaker dependence of A_{xg} on \aleph does not allow us to provide any useful constraints on the evolutionary parameter. This is expected however since, by construction, Equation 17 is normalized by the amplitude of the full $18 < B < 23$ dataset and therefore dominated by these fainter galaxies.

The errors on δA_{xg} suggest values of \aleph in the range $-1.37 < \aleph < 0.58$. This global parameter was defined $\aleph = \gamma - \epsilon + q - 5$ where q describes the evolution of the X-ray emissivity as a function of redshift (Equation 8) and γ and ϵ characterise the clustering properties of the galaxy population (see Equation 10). We have assumed that the

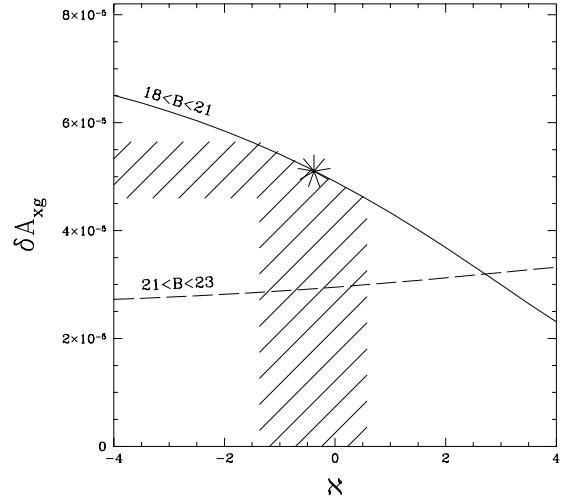


Figure 7. Showing the expected relationship between the amplitude of the cross-correlation function W_{xg} and the evolutionary parameter \aleph for brighter $18 < B \leq 21$ galaxies (solid upper line) and the fainter $21 \leq B < 23$ galaxies (lower dashed line). The shaded region displays the 1σ error bounds on the *measured* amplitude for the brighter galaxies and the corresponding range of \aleph .

latter two quantities are relatively well defined in comparison with the parameter q and adopt the values $\gamma = 1.8$ and $\epsilon = 0$. This value of ϵ allows the galaxy evolution model of Roche et al (1996a) to simultaneously fit the faint galaxy number counts and the galaxy clustering. This leads to values of $q = 2.82 \pm 0.98$ and thus a best estimate for the evolution of the X-ray emissivity due to galaxies:

$$\rho_x(z) = \rho_o(1+z)^{2.82 \pm 0.98} \quad (18)$$

Using a spectral index of $\alpha_x \sim 0.6$ (Almaini et al. 1996) we can obtain our best estimate for the X-ray luminosity evolution of faint galaxies:

$$L_x \propto (1+z)^{3.22 \pm 0.98} \quad (19)$$

which is very similar to the X-ray evolution of AGN. Similar forms have been obtained by considering the luminosity function of individually identified X-ray luminous galaxies at much brighter fluxes (Griffiths et al. 1995, Boyle et al. 1995a).

Since the $N(m, z)$ of Roche et al. (1996a) places the faint blue galaxy population at relatively high redshift, it might be argued that the strong evolution we have detected here is due to our particular choice of galaxy evolution model. We have therefore repeated the analysis using the model of Efstathiou (1995), following TL96, which assumes a much more local population of faint galaxies. Although the mean redshifts are lower, this model uses a much smaller correlation radius ($r_0 = 2 h^{-1} \text{Mpc}$) with comoving clustering evolution ($\epsilon = -1.2$) rather than the stable model we have used in this paper ($\epsilon = 0$). The end result is a very similar galaxy-galaxy angular autocorrelation. Even with this model we still obtain evidence for strong evolution in X-ray luminosity ($L_x \propto (1+z)^{3.5 \pm 1.2}$).

3.8 The X-ray volume emissivity of faint galaxies

With an estimate for the X-ray evolution we may now estimate the volume emissivity due to faint galaxies using Equation 11. First we require the amplitude of the observed angular cross-correlation function $W_{xg}(\theta)$ (Figure 4). As before, fitting the functional form given by Equations 14 and 15, we obtain (measuring θ in radians):

$$A_{xg} = 3.60 \pm 0.27 \times 10^{-5} \quad (20)$$

The mean intensity of the unresolved XRB from the 3 deep ROSAT fields used here is $\bar{I} = 1.59 \pm 0.2 \times 10^{-8} \text{ erg s}^{-1} \text{ cm}^{-2} \text{ sr}^{-1}$ and $\bar{N} = 2.64 \times 10^7 \text{ galaxies sr}^{-1}$ in the magnitude range $18 < B < 23$. Putting all of this together we may now obtain the local X-ray volume emissivity via Equation 11 (using $q_0 = 0.5$, $\Lambda = 0$):

$$\rho_o \simeq 3.02 \pm 0.23 \times 10^{38} \text{ h ergs}^{-1} \text{ Mpc}^{-3} \quad (21)$$

It should be emphasized however that this estimate relies on very specific assumptions about the distribution and clustering properties of the galaxy population. In particular since $\rho_o \propto r_o^{-\gamma}$ (from Equation 11), a less clustered model with $r_o < 4.4 h^{-1} \text{ Mpc}$ will **increase** the required local emissivity. Such weak clustering would be required in models which place most faint galaxies at relatively low redshift (eg. Efstathiou et al 1995). Recent deep spectroscopic work seems to confirm the existence of a significant high redshift population however (eg. Cowie et al. 1996).

3.9 The contribution of faint galaxies to the unresolved XRB

We may now obtain a rough estimate the total contribution of the $18 < B < 23$ catalogue galaxies to the unresolved XRB by integrating the volume emissivity out to the median redshift of the sample, $z = 0.45$. Modifying Equation 9 gives the following expression for the contribution to the sky intensity per unit solid angle:

$$\begin{aligned} \Delta \bar{I}_g &= \omega \int_{z=0}^{z=0.45} \frac{\rho_g(z)}{4\pi r_l^2(z)} dv(z) \\ &= 3.6 \pm 0.5 \times 10^{-9} \text{ ergs}^{-1} \text{ cm}^{-2} \text{ sr}^{-2} \end{aligned} \quad (22)$$

This accounts for $23 \pm 3\%$ of the unresolved X-ray background, where the error is derived entirely from the uncertainty in the observed X-ray quantities, $W_{xg}(\theta)$ and \bar{I} .

To determine the “total” galaxy contribution to the XRB we simply extrapolate Equation 22 to the faintest galaxies at arbitrarily high redshifts. This process becomes increasingly uncertain as we extend the redshift distribution beyond the limit of our sample at $B = 23$, but nevertheless by integrating to $z = 2$ we formally obtain $\sim 80 \pm 20\%$ of the unresolved $0.5 - 2.0 \text{ keV}$ XRB, which is $\sim 40 \pm 10\%$ of the total XRB intensity. Given the uncertainties already inherent in this procedure it will probably suffice to say that galaxies can produce a significant fraction of the XRB at least as high as the contribution from QSOs.

3.10 Blue and red galaxies

To constrain the colour and type of galaxies producing the cross-correlation signal we use R band plates to separate the

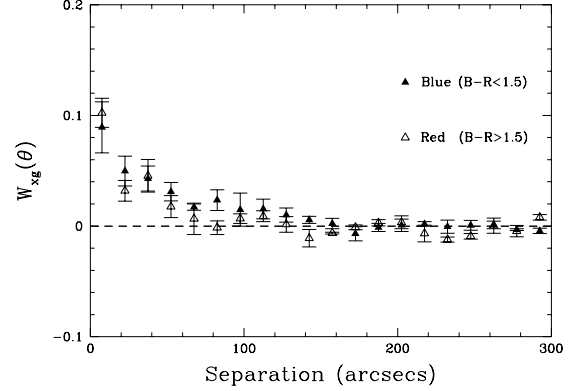


Figure 8. The cross-correlation function $W_{xg}(\theta)$ of galaxies with the unresolved $0.5 - 2.0 \text{ keV}$ XRB, separating blue from red galaxies and combining the results from three ROSAT fields.

sample into blue and red subsets, dividing at $B - R = 1.5$. The cross-correlations were then carried out separately for each dataset. The results (Figure 8) show no significant difference in the cross-correlation amplitudes, suggesting that galaxies of all morphological types are contributing to the signal. Blue galaxies at these magnitudes are known to be more weakly clustered however, with autocorrelation amplitudes lower by a factor of ~ 4 at these magnitudes (Roche et al. 1996a) and hence the enhancement in $W_{xg}(\theta)$ due to clustering will be significantly lower for the blue subset. Thus the typical X-ray luminosities may be higher for the blue galaxies (by $\sim 50\%$), but a more careful analysis is required to prove this since the $N(m, z)$ distribution for blue and red galaxies may be significantly different.

4 FUTURE PROSPECTS

Having established the existence of a population of highly luminous X-ray galaxies, the next intriguing question is the origin and nature of this activity. Boyle et al. (1995b) have obtained high resolution optical spectroscopy for a selection of individual X-ray galaxies at much brighter magnitudes which suggests a mixture of starburst and Seyfert 2 activity. In many cases however the classification was ambiguous. Type 2 AGN provide a natural explanation since the expected X-ray absorption can readily reproduce the flat spectra of the XRB (Comastri et al. 1995, Madau et al. 1994). At least two of the brighter X-ray galaxies identified in Almaini et al. (1996) show clear evidence of X-ray obscuration. The discovery of a high redshift counterpart to this population adds further credence to this possibility (Almaini et al. 1995). Explaining the XRB with an AGN population may be difficult however since QSOs are strongly clustered and may violate the upper limits of the isotropy of the XRB (Georgantopoulos et al. 1993, Soltan & Hasinger 1994). It

may also be difficult to reproduce the smooth, featureless spectrum of the hard XRB as observed with ASCA (Gendreau et al. 1995).

Starburst activity is another possible explanation. There have been suggestions that massive X-ray binaries formed in the wake of star formation in early, low metallicity epochs may provide a strong source of hard X-ray emission (Griffiths and Padovani 1990, Treyer et al. 1992). A third explanation has emerged recently which describes dead quasars residing in seemingly normal galaxies as remnants of an earlier, more active epoch (Di Matteo & Fabian 1997). The low accretion efficiency may give rise to advection dominated accretion and a two temperature gas in which the ions are much hotter than the electrons. The electron temperature saturates at ~ 100 keV and gives rise to Bremsstrahlung radiation. A superposition of many such sources over a range of redshifts can then provide a good fit to the XRB.

Infra-red spectroscopy may provide a conclusive test of the AGN hypothesis by allowing us to see through the obscuring dust to detect broad emission lines in moderately obscured AGN. If the nuclei are heavily obscured the infra-red emission may also be obliterated, but in this scenario it is difficult to produce the soft X-ray flux we observe with *ROSAT* without a very large $\sim 10\%$ scattered component. Spectropolarimetry may allow us to detect broad emission lines scattered around the obscuring medium and into our line of sight. Deep radio and far infra-red observations may allow us to detect the signatures of starburst activity. The ion supported tori model of Di Matteo & Fabian should also be tested by searching for the predicted distinctive emission peak at short radio wavelengths. Further observations are clearly required to distinguish between these competing explanations.

5 SUMMARY AND CONCLUSIONS

By cross-correlating faint galaxy catalogues with unidentified X-ray sources a strong (4.2σ) signal was detected indicating that individual galaxies with magnitude $B < 23$ account for $20 \pm 7\%$ of all X-ray sources to a limiting flux of $\sim 4 \times 10^{-15} \text{ erg s}^{-1} \text{ cm}^{-2}$ in the $0.5 - 2.0$ keV band. This builds on the results of Roche et al. (1995) who found a significant signal in cross-correlation with brighter $B < 21$ galaxies, attributing $\sim 6\%$ of the X-ray sources to these brighter objects. Scaling the 20% galaxy fraction by the median flux of the unidentified X-ray sources leads to $\sim 4\%$ of the total XRB intensity.

To probe deeper we cross-correlate with individual photons in the remaining unresolved XRB images. Significant signals were obtained on all 3 deep *ROSAT* images, each of similar amplitude, independently confirming the results obtained by Roche et al. (1995). To translate these cross-correlations into a total fraction of the unresolved XRB a specific description of the galaxy population is adopted, modelling the evolution, number density and clustering properties of the faint blue galaxy population using the formalism developed by TL96. We modify this formalism to allow for the effect of finite cell sizes and the effect of the *ROSAT* point-spread function. By comparing the theoretical XRB cross-correlation with the observed signal an estimate for the local X-ray volume emissivity was obtained at

$\rho_o \simeq 3.02 \pm 0.23 \times 10^{38} \text{ h ergs}^{-1} \text{ Mpc}^{-3}$ ($q_o = 0.5$, $\Lambda = 0$). Scaling the implied X-ray to optical luminosity ratio by the integrated blue band flux leads to an estimate that $B < 23$ galaxies account for $\sim 20\%$ of the unresolved XRB. Extrapolation to high redshift ($z = 2$) suggests that faint galaxies can account for $\sim 40 \pm 10\%$ of the total XRB at 1 keV. These estimates have a strong dependence on the assumed distribution and clustering properties of the faint galaxy population.

When the optical galaxy catalogue is separated into blue and red subsets, dividing at $B - R = 1.5$, no significant difference is found in the cross-correlation with the XRB. This would suggest that a mixture of galaxy colours and morphologies contribute to the observed signal. Given that red galaxies are more strongly clustered at these magnitudes, this may also indicate that bluer galaxies are intrinsically more X-ray luminous.

To constrain the evolution of X-ray emissivity with redshift, separate cross-correlations were carried out with two magnitude slices of the galaxy population. The resulting difference in amplitude suggests that faint galaxies evolve strongly with redshift such that:

$$L_x \propto (1 + z)^{3.22 \pm 0.98} \quad (23)$$

which represents the first evidence that the X-ray emission from faint blue galaxies evolves as strongly as AGN. Similar results have been obtained by analysing the brightest narrow emission-line galaxies emerging from deep *ROSAT* exposures (Griffiths et al. 1996, Boyle et al. 1995a).

Combined with recent findings which suggest that X-ray luminous galaxies have hard X-ray spectra, it now seems established beyond doubt that a population of faint galaxies, or some processes associated with them, are emitting vast amounts of X-ray radiation which may finally solve the puzzling origin of the X-ray background.

ACKNOWLEDGMENTS

OA was funded by a PPARC postdoctoral fellowship. OA thanks Marie Treyer, Alexandre Refregier and Ofer Lahav for their considerable help with this work.

REFERENCES

- Almaini O., Boyle B.J., Griffiths R.E., Shanks T., Stewart G.C. & Georgantopoulos I., 1995, MNRAS 277, L31
- Almaini O., Shanks T., Boyle B.J., Griffiths R.E., Roche N., Stewart G.C. & Georgantopoulos I., 1996, MNRAS 282, 295
- Boyle B.J., Fong R., Shanks T. & Peterson B.A. 1990. MNRAS, 243, 1
- Boyle B.J., Jones L.R., & Shanks, T., 1991 MNRAS 251, 482
- Boyle B.J., McMahon R.G., Wilkes B.J., & Elvis M., 1995a, MNRAS 272, 462
- Boyle B.J., McMahon R.G., Wilkes B.J., & Elvis M., 1995b, MNRAS 276, 315
- Carballo R. et al. 1995, MNRAS 277, 1312
- Carrera F.J. et al. 1995, MNRAS 275, 22
- Comastri A., Setti G., Zamorani G. & Hasinger G., 1995, A&A, 296, 1
- Cowie et al. 1996, AJ 112, 839
- mastri A., Setti G., Zamorani G. & Hasinger G., 1995, AJ in press

- Di Matteo T. & Fabian A.C., 1997 MNRAS In press
- Gendreau K.C. et al, 1995, Publ. Astron. Soc. Japan, 47, L5-L9
- Georgantopoulos I., Stewart G.C., Shanks T., Griffiths R.E., & Boyle B.J., 1993, MNRAS 262, 619
- Georgantopoulos I., Stewart G.C., Shanks T., Griffiths R.E., & Boyle B.J., 1996, MNRAS 280, 276
- Griffiths R.E. & Padovani P. 1990, ApJ 360, 483
- Griffiths R.E., Georgantopoulos I., Boyle B.J., Stewart G.C., Shanks T., Della Ceca R., 1995a, MNRAS 275, 77
- Griffiths R.E., Della Ceca R., Georgantopoulos I., Boyle B.J., Stewart G.C., Shanks T. & Fruscione A., 1996, MNRAS 281, 71
- Hasinger G., Turner J.T., George I.M., Boese G., 1992, GSFC Calibration Memo CAL/ROS/92-001
- Hasinger G., Burg R., Giacconi R., Hartner G., Schmidt M., Trümper J., Zamorani G., 1993, A&A, 275, 1
- Lahav O. et al. 1993, Nature 364, 693
- McHardy I. et al., 1995, Spectrum 6, 11
- Metcalf N., Shanks T., Fong R., Jones L.R., 1995, MNRAS 273, 257
- Miyaji T. et al. 1994 ApJ 393, 134
- Morisawa K. et al. A&A 236, 299
- Mushotzky R.F., Done C., Pounds K.A., 1993, Ann. Rev. Astr. Ap., 31, 717
- Plucinsky P.P., Snowden S.L., Briel U.G., Hasinger G., Pfeffermann E., 1993, ApJ 418, 519
- Refregier A., Helfand J.D. & McMahon R.G., 1997, ApJ 477, 58
- Roche N., Shanks T., Georgantopoulos I., Stewart G.C., Boyle B.J., & Griffiths R.E., 1995a, MNRAS 273, L15
- Roche N., Shanks T., Metcalfe, N., Fong, R., 1996a, MNRAS 280, 397
- Roche N., Griffiths R.E., Della-Ceca R., Shanks T., Boyle B.J., Georgantopoulos I. & Stewart G.C., 1996b, MNRAS In Press
- Romero-Colmenero E., Branduardi-Raymont G., Carrera F.J., Jones L.R., Mason K.O., Mc Hardy I.M. & Mittaz J.P.D., 1996, MNRAS 282, 94
- Shanks T., Georgantopoulos I., Stewart G.C., Pounds K.A., Boyle B.J. & Griffiths R.E., 1991 Nat 353, 315
- Shanks T., Boyle B.J., Griffiths R.E., Stewart G.C., Georgantopoulos I., Almaini O., Roche N. 1997 MNRAS submitted
- Snowden S.L., Freyberg M.J., 1993, ApJ 404, 403
- Soltan A., Hasinger G., 1994 A&A 288, 77
- Stewart G.C., Georgantopoulos I., Boyle B.J., Shanks T., Griffiths R., 1994, New Horizon Of X-ray Astronomy - first results from ASCA, p331, eds. F. Makino and T. Ohashi, Universal Academy Press, Tokyo
- Treyer M.A. et al. 1992, A&A 264, 11
- Treyer M.A. & Lahav O. 1996 MNRAS 280, 469
- Tyson J.A. et al. 1988, AJ 96, 1
- Vikhlinin A., Forman W., Jones C. & Murray S., 1995 ApJ 451, 564